Electrochemical characterization of Li10SnP2S12: An electrolyte or a negative electrode for solid state Li-ion batteries?

Ilyas Tarhouchi, Philippe Vinatier, Michel Ménétrier, Virginie Viallet

Electrochemical characterization of $Li_{10}SnP_2S_{12}$: An electrolyte or a negative electrode for solid state Li-ion batteries?

Ilyas Tarhouchi [a,b,c], Virginie Viallet [b,c], Philippe Vinatier [a,c], Michel Ménétrier [a,c,*]

[a] CNRS, Univ. Bordeaux, Bordeaux INP, ICMCB UPR9048, F-33600 Pessac, France
[b] Laboratoire de Réactivité et de Chimie des Solides, Université de Picardie Jules Verne, CNRS UMR#7314, F-80039 Amiens, France
[c] RS2E, Réseau Français sur le Stockage Electrochimique de l'Energie, CNRS FR#3459, F-80039 Amiens, France

Keywords:
LGPS structure
Sulfide
Solid electrolyte
Electrochemical properties
Conversion reaction

A B S T R A C T

$Li_{10}SnP_2S_{12}$, the tin analogue of the $Li_{10}GeP_2S_{12}$ superionic conductor is characterized. Rietveld refinement of cap illary powder XRD confirms that the material provided by NEI Corp. is mainly composed of $Li_{10}SnP_2S_{12}$ with LGPS structure, with some Li_2SnS_3 impurity. Very strong reactivity at low voltage and vs. Li metal is shown by imped ance measurements using Au and Li electrodes, as well as 3 electrode cyclic voltammetry. Galvanostatic mea surements in half cells with liquid and solid electrolytes confirm that $Li_{10}SnP_2S_{12}$ reacts with respectively 16 and 8 lithium per mole of tin below 0.5 V vs. Li^+/Li, most probably following a conversion/alloying reaction. Mak ing use of this reactivity, we tested the concept of a $LiCoO_2/Li_{10}SnP_2S_{12}$ cell, were the electrolyte also acts as neg ative electrode at the contact with the negative current collector. 0.5 Li can be deintercalated from such cells, with very poor reversibility as probably hampered by the conversion/alloying reaction in the solid state, at least with a non optimized electrode formulation. Although the voltage slowly but strongly relaxes when opening the circuit suggesting propagation of the reaction from the negative electrode to the electrolyte, it does not seem to reach the positive since no short circuit was observed.

1. Introduction

Among all electrical energy storage technologies, Li ion batteries be come more and more favored, since their high energy densities are of first interest for portable devices, electrical vehicles or smart grids de velopment. However, safety issues remain, since organic liquid electro lyte currently used in such batteries can leak (with hydrofluoric acid emission), or ignite [1]. Development of Li all solid state batteries can be considered as a possible alternative, since they are based on non flammable solid electrolytes, in place of organic liquid electrolytes.

The solid electrolyte should exhibit key properties: low electronic conductivity, chemical stability vs. the electrode materials, wide electro chemical stability window and high ionic conductivity. The latter was considered as the main issue for the development of all solid state bat teries, since the best solid electrolytes exhibited an ionic conductivity at room temperature of 10^{-3} S·cm^{-1}, which is less than that of liquid electrolytes (10^{-2} S·cm^{-1}).

Kanno published recently a new solid electrolyte, $Li_{10}GeP_2S_{12}$, exhibiting a room temperature ionic conductivity of 1.2×10^{-2} S·cm^{-1}, comparable to or higher than ionic conductivities of organic electrolytes used in Li ion batteries [2]. It crystallizes in a tetragonal LGPS structure ($P4_2/nmc$ space group) with isolated (Ge/P)S_4 tetrahedra, where phosphorus occupies 2*b* sites (or 2*a* sites de pending on the origin chosen for the space group) with 100% occupancy and share the 4*d* site with Ge with (nominally) 50% occupancy. This LGPS structure, later confirmed by single crystal XRD [3], is different from the one published a few years before for the $Li_{10}GeP_2S_{12}$ composi tion: in the $Li_{4-x}Ge_{1-x}P_xS_4$ solid solution with Li_4GeS_4 and Li_3PS_4 end members, Kanno had indeed presented materials which crystallize in an orthorhombic thio LiSICON structure (γ Li_3PO_4 type) with different monoclinic superlattice modifications depending on x [4].

Computation results on $Li_{10}MP_2S_{12}$ (M = Si, Ge, Sn) with LGPS struc ture predicted these solid electrolytes to decompose into Li_3PS_4 and Li_4MS_4, and thus the "tetragonal" LGPS structure for $Li_{10}MP_2S_{12}$ compo sition to be metastable, although weakly. However, an ordered structure was necessarily considered for the calculation and resulted in a *P*1 space group, which is different from the tetragonal LGPS obtained experimen tally [5,6].

Very recently, Kanno reported an $Li_{4-x}Ge_{1-x}P_xS_4$ ($0.5 \le x \le 0.65$) solid solution range for which materials have a pure LGPS structure, with different Ge/P ratios in the 4*d* site depending on the composition [7]. For other $Li_{4-x}M_{1-x}P_xS_4$ (M = Si, Sn), similar solid solution ranges crystallizing in a pure LGPS structure were also reported, but for differ ent compositions [8].

Cyclic voltammetry of selected Ge, Si and Sn LGPS type materials using a pellet with a gold sputtered working electrode facing a lithium

* Corresponding author at: ICMCB-CNRS, 87 Avenue Schweitzer, F-33600 Pessac Cedex, France.
E-mail address: michel.menetrier@icmcb.cnrs.fr (M. Ménétrier).

counter and reference electrode was reported [2,8]. These materials were thus presented to be stable up to 5 V vs. Li^+/Li (no decomposition peaks being observed), making these solid electrolytes suitable for high energy density batteries application. Nevertheless, the calculation results predicted all $Li_{10}MP_2S_{12}$ with LGPS structure to be unstable at 0 V and 5 V vs. Li^+/Li [6].

$Li_{10}SnP_2S_{12}$ has been made available commercially by NEI Corp., even before the first preparation report of $Li_{10}SnP_2S_{12}$ by Bron et al. [9]. In the latter report, X ray diffraction confirms single crystals with this composition crystallizing in the LGPS structure, and the ionic bulk conductivity of 7×10^{-3} S·cm^{-1} at room temperature is in agreement with previous calculations [6].

In the present study, we describe a characterization of the commercial $Li_{10}SnP_2S_{12}$ material. Rietveld refinement of X ray diffractograms confirms the tetragonal LGPS structure with some Li_2SnS_3 impurity; impedance measurements show an unexpected effect of the measurements itself; three electrode cyclic voltammetry reveals the narrow electrochemical stability window of $Li_{10}SnP_2S_{12}$ and especially at low potential. We finally propose the concept of a solid state battery using this material both as solid electrolyte and as negative electrode material. We note that the concept of using an LGPS type material as electrolyte and as active electrode was actually very recently proposed by Han et al. while we were investigating it independently [10]. These authors even propose that $Li_{10}GeP_2S_{12}$ also act as positive electrode; however, they did not address the behavior upon long relaxation.

2. Experimental

$Li_{10}SnP_2S_{12}$ was purchased from NEI Corporation and is referred to as $Li_{10}SnP_2S_{12}$ NEI (nominally >95% purity).

Based on previous studies [11], Li_2SnS_3 was prepared as follows: the precursors Li_2S (Sigma Aldrich, 99.9% of purity), Sn (Sigma Aldrich, 99.8% of purity) and sulfur are mixed and ground in a mortar in stoichiometric proportions. The powder mixture is placed in a vitreous carbon crucible, which is then placed in a silica tube. All these operations are carried out in a glove box under Ar atmosphere. The tube is sealed under vacuum and heat treated at 750 °C during 24 h.

X ray diffraction patterns were obtained using a Panalytical Empirean diffractometer operating with Cu $K\alpha_1\alpha_2$ radiation (λ_1 = 1.5406 Å and λ_2 = 1.5443 Å) in capillary configuration (transmission) with 0.2 mm diameter capillaries. Le Bail and Rietveld refinements of the XRD pattern were performed using the Fullprof suite [12].

Impedance measurements were carried out using a Solartron 1260 analyzer on pellets (Ø 13 mm 5 tons/370 MPa). Depending on the experiment, a heat treatment (500 °C during 12 h in an evacuated glass ampoule) was applied or not on the pellet, as indicated in each case. Gold blocking electrodes were sputtered on each face of the pellets using a device directly opening into the dry box. Measurements were carried out between 10 MHz and 1 Hz or between 10 MHz and 10 kHz, with an amplitude of 20 mV. For the temperature dependence study, impedance diagrams were measured every 5 °C once the oven temperature was stable (variation lower than 0.5 °C during 10 min) between 25 °C and 110 °C. For the Arrhenius plots, the temperature used is the one measured by a sensor in the measuring cell very close to the sample.

Impedance measurements were also carried out on cold pressed pellets (Ø 13 mm 5 tons/370 MPa), with Li foils as electrodes. The measurements were carried out at different times between $t = t_0$ and $t = t_0 + 94$ h and for frequencies between 10 MHz and 1 Hz with an amplitude of 50 mV.

Electrochemical stability was characterized by cyclic voltammetry using a 3 electrode set up: on one side of the solid electrolyte pellet, a gold working electrode is sputtered on half the surface. On the other side of the pellet, a gold counter electrode is sputtered on the entire surface. A thin piece of a pressed mixture of Ag_3SI (prepared as reported by Takahashi and Yamamota [13] and Ag (Sigma Aldrich, 99.9% of purity)) is used as reference electrode and is kept in contact on the non sputtered part of the pellet, next to the working electrode. The measured potential of the reference electrode was 2.11 V vs. Li^+/Li in agreement with earlier work [14]. Using a VMP galvanostat potentiostat (Biologic), cyclovoltammograms were performed at 20 mV·s^{-1} between −2 V and 5 V vs. Ag_3SI/Ag, starting with anodic or cathodic sweep.

Liquid electrolyte coin cells (14 mm diameter) were built using 1 M LiTFSI in TEGDME/1,4 dioxane (Sigma Aldrich) as electrolyte soaked in a Celgard plus Viledon separator, a Li metal foil as negative, and the positive was a mixture of the $Li_{10}SnP_2S_{12}$ or Li_2SnS_3 active material (80 mass%), Super P carbon (15 wt%) as conducting additive, and PTFE (Sigma Aldrich 5 wt%) as binder. All solid state cells with $Li_{10}SnP_2S_{12}$ NEI (or Li_2SnS_3) used as active positive electrode material were built as follows: composite electrodes were prepared by mixing in a mortar 40 mg of $Li_{10}SnP_2S_{12}$ NEI (or Li_2SnS_3), 5 mg of Vapor Grown Carbon Fiber (VGCF Shoma Denko) and 60 mg of Li_6PS_5Cl prepared as reported by Boulineau et al. [15]. The batteries were assembled by cold pressing (Ø 10 mm, 5 tons/370 MPa) 10 mg of composite as positive electrode (15 mg for Li_2SnS_3), 80 mg of Li_6PS_5Cl as solid electrolyte, and a Li foil as negative electrode. Using a VMP galvanostat potentiostat (Biologic), galvanostatic measurements were carried out at 64 μA·cm^{-2} (starting with discharge) with potential limits at 0.1 V and 5 V vs. Li^+/Li. The measurements were performed in argon atmosphere using the device described in Fig. 1, which maintains a pressure on the all solid state cell while cycling.

For all solid state cells with $Li_{10}SnP_2S_{12}$ NEI as negative electrode and electrolyte, composite electrodes are prepared by mixing in a mortar 40 mg of $LiCoO_2$, 60 mg of $Li_{10}SnP_2S_{12}$ NEI and 5 mg of VGCF for the positive electrode composite and 100 mg of $Li_{10}SnP_2S_{12}$ NEI and 5 mg of VGCF for the negative electrode composite. 10 mg of positive electrode composite, 80 mg of $Li_{10}SnP_2S_{12}$ NEI and 10 mg of negative electrode composite are cold pressed (Ø 10 mm, 5 tons 375 MPa) to form an all solid state battery, in the same device as described above. Galvanostatic measurements were carried out at 64 μA·cm^{-2} (starting with charge) with voltage limits at 3.7 V and 2 V.

3. Results and discussions

3.1. Structural characterization

Fig. 2 shows the XRD pattern of $Li_{10}SnP_2S_{12}$. The sloping baseline is due to the capillary Debye Scherer setup used. The crystal structure published by Bron et al. was used as starting point for Rietveld refinement of this powder pattern [9]. Global although not perfect agreement was achieved by considering the presence of a second minority phase,

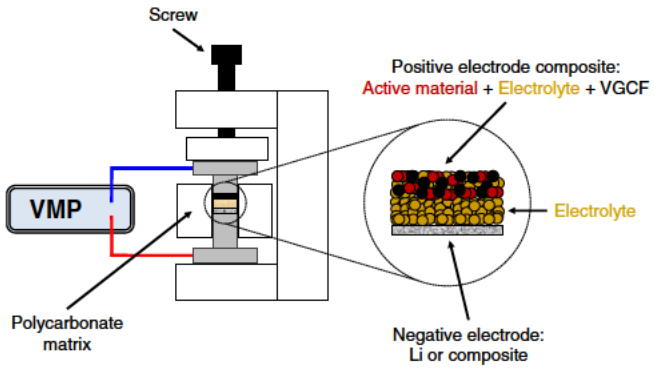

Fig. 1. Device for all-solid state cells.

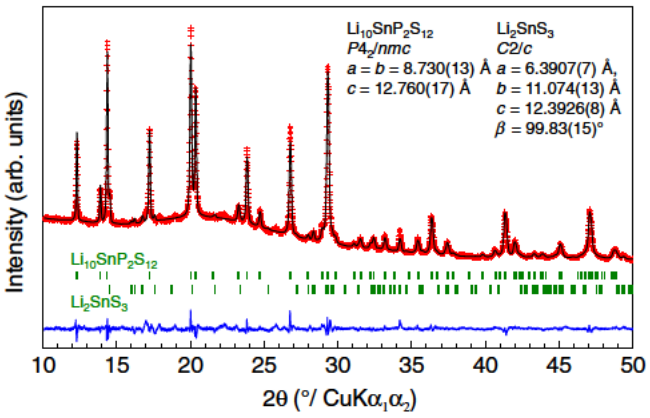

Fig. 2. Capillary XRD pattern of $Li_{10}SnP_2S_{12}$-NEI and Rietveld refinement based on the tetragonal LGPS structure proposed by Bron et al. [9].

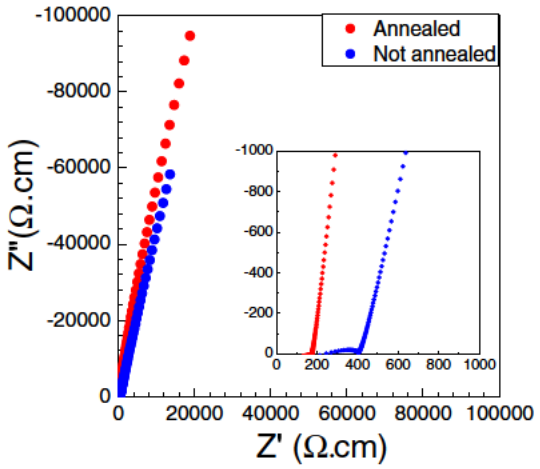

Fig. 3. AC impedance diagrams for pristine and annealed pellets of $Li_{10}SnP_2S_{12}$ with sputtered gold electrodes (1 MHz–1 Hz frequency sweep).

namely Li_2SnS_3 (6 wt%). Table 1 shows the result of the refinement. We note that this impurity is also detectable in the powder diffraction pattern by Bron et al. but was not mentioned. Therefore, $Li_{10}SnP_2S_{12}$ NEI is mainly composed of $Li_{10}SnP_2S_{12}$ with LGPS structure ($P4_2/nmc$) with cell parameters, $a = b = 8.730(13)$ Å, $c = 12.760(17)$ Å close to those proposed by Bron et al. for a single crystal ($a = b = 8.7057(4)$ Å, $c = 12.7389(9)$ Å) [9]. As shown in Table 1, our refinement of the Sn/P occupation factors in site 4*d* leads to a 0.51/0.49 ratio (i.e. $Li_{10.03}Sn_{1.03}P_{1.97}S_{12}$). This leads to a slightly better fit than with fixed 0.5/0.5 occupation factors. We note in this respect that Bron et al. do not mention the refinement of the occupation factors, and give a 0.5/0.5 value in their cif file [9]. Kuhn et al. refined the occupation factors from their powder diffractogram, leading to 0.47/0.53 [16]. Finally, Hori et al. apparently use the experimental composition of the starting mixture for the synthesis as fixed occupation factors [8]. We also note that indexing using Le Bail full pattern matching based on a thio LiSICON Ge type II structure ($P2_1/m$, $a = 13.396(3)$ Å, $b = 22.947(6)$ Å, $c = 18.2009(15)$ Å, $\beta = 92.562(14)°$) [4] leads to a poor agreement, despite the large number of reflections in the model, even when taking into account the presence of Li_2SnS_3 as impurity (see Appendix A Fig. A1). There is therefore no ambiguity between the orthorhombic thio LiSICON type and the tetragonal LGPS type structure for this material.

3.2. Ionic conductivity

Since pressed pellets are required to measure the ionic conductivity of the material, we have first investigated the effect of annealing of pellets obtained by room temperature pressing at 3.77 $t \cdot cm^{-2}$. Annealing at 500 ° C for 12 h does not modify significantly the compactness which is 75% based on the theoretical density of ideal $Li_{10.03}Sn_{1.03}P_{1.97}S_{12}$ with the cell parameters obtained by our Rietveld refinement. Fig. 3 shows the room temperature impedance diagrams (1 MHz 1 Hz frequency sweep) of unannealed and annealed pellets with sputtered blocking gold electrodes. For the annealed pellet, only the capacitive effect of the electrodes is observed even at 1 MHz, leading to a conductivity of $5 \cdot 10^{-3}$ $S \cdot cm^{-1}$ at RT, consistent with the room temperature data reported by Bron et al., and with the calculations by Ong et al. [6,9]. However, the diagram for the unannealed pellet exhibits in addition a depressed semi circle, the beginning of which is consistent with the resistance for the annealed pellet, although high frequency measurements (>1 MHz in the present case) are always perturbed by artifacts from the experimental setup. It therefore appears that an additional contribution from intergrain effects exists before annealing. This contribution is no longer visible at room temperature in our frequency range after annealing, which suggests that, although the compactness of the pellet was not modified, annealing improves the intergrain contacts. However, we note that by decreasing the temperature, Bron et al. were able to observe an intergrain phenomenon in their annealed pellets of $Li_{10}SnP_2S_{12}$ [9]. We note also that in most reports of LGPS type materials, annealing of the pellets is carried out before conductivity measurements, whereas Kato et al. state that annealing does not change significantly the conductivity for $Li_{10}GeP_2S_{12}$, but impedance diagrams are not shown [17].

The temperature dependence of the impedance diagrams was studied on annealed pellets in the 25 °C ≤ T ≤ 110 °C range. The diagrams measured during the temperature increase (Fig. 4a) show only the

Table 1
Atomic positions and Rietveld refinement parameters of the $Li_{10}SnP_2S_{12}$-NEI XRD pattern based on the tetragonal LGPS structure proposed by Bron et al. [9].

$Li_{10}SnP_2S_{12}$		Radiation: Cu			$\lambda_1 = 1.54056$ Å	$\lambda_2 = 1.54439$ Å
$P4_2/nmc$			$R_{Bragg} = 5.14\%$		$\chi^2 = 2.72$	
$a = b = 8.730(13)$ Å		$c = 12.760(17)$ Å		$Z = 2$	$V = 972.43(2)$ Å^3	
Atom	Wyckoff position	Occupancy	*x* / *a*	*y* / *b*	*z* / *c*	B_{iso} (Å^2)
Sn1	4*d*	0.515(1)	¼	¼	1.06364(12)	2.43(5)
P1	4*d*	=1 occ.(Sn1)	=*x* / *a* (Sn1)	=*y* / *b* (Sn1)	=*z* / *c* (Sn1)	=B_{iso} (Sn1)
P2	2*a*	1	¾	¼	¾	1.68(13)
S1	8*g*	1	0.56046(18)	¼	0.84162(17)	2.96(8)
S2	8*g*	1	¼	0.4651(2)	0.65570(17)	2.70(7)
S3	8*g*	1	¼	0.4551(2)	0.95734(15)	2.52(8)

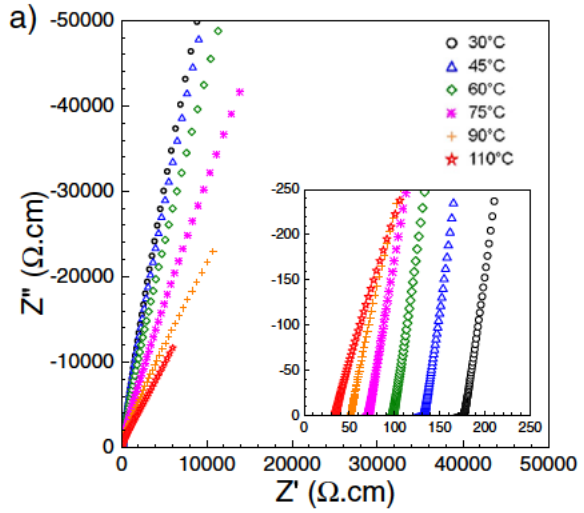

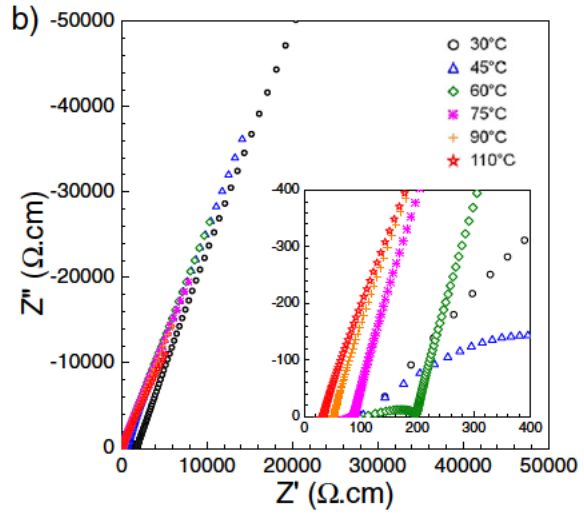

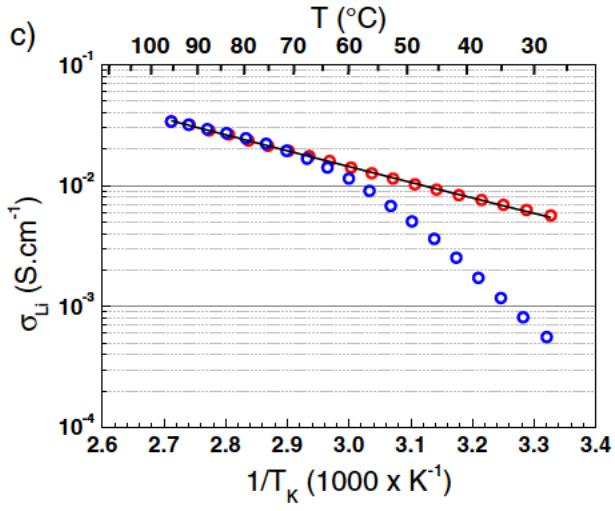

Fig. 4. a) Selected impedance diagrams of an annealed $Li_{10}SnP_2S_{12}$ pellet with sputtered gold electrodes between room temperature and 110 °C. b) Selected impedance diagrams of an annealed $Li_{10}SnP_2S_{12}$ pellet with sputtered gold electrodes between 110 °C and room temperature c) resulting global conductivities in Arrhenius coordinates.

electrode capacitive effect, although with a slight degradation of the blocking effect upon heating (less vertical low frequency branch). Even though the extrapolated dc resistance results from bulk and intergrain contributions, the corresponding global conductivity follows an Arrhenius behavior as shown in Fig. 4c with an activation energy of 0.26 eV, typical of fast ionic conductors, in agreement with previous reports [6,9]. However, the impedance diagrams shown in Fig. 4b recorded during the temperature decrease clearly show the appearance of a new phenomenon for temperatures lower than 60 °C. Obviously, a strong intergrain or interfacial phenomenon takes place before the electrode blocking effect. Therefore, if we plot a global conductivity determined at the intercept of the latter, the data no longer follow an Arrhenius behavior (Fig. 4c), as expected considering that the resistance measured in such a way includes different phenomena, and the global conductivity appears much lower at lower temperatures. No change however was observed in the XRD signature of the material after this measurement.

In order to assess whether the impedance measurements can be the cause of the degradation, we have carried out a similar series of variable temperature measurements in a narrower (10 MHz 10 kHz) frequency range on a fresh pellet. As shown in Fig. 5, the room temperature impedance diagram before heating is of course identical to that discussed above, except that the blocking electrode branch is interrupted at 10 kHz instead of extending to much lower frequency (1 Hz). More interestingly, the diagram recorded after the heating/cooling process shows appearance of a similar phenomenon, but with a significantly smaller magnitude than when sweeping to lower frequencies. These data thus reveal that the AC voltage with 20 mV magnitude applied to the cell at temperatures ranging from RT to 110 °C creates this new intergrain/interface phenomenon. It is therefore logically stronger for the lower frequency sweep since the AC voltage is then applied for a much larger number of periods, each lasting in addition much longer. The temperature at which this phenomenon actually appears cannot really be determined, since in any case is it not visible at temperatures higher than 70 °C (Fig. 4b). The frequencies at which it can be observed at these temperatures probably exceed the capabilities of our experimental setup (1 MHz). However, it is clear that this reaction is significant only at elevated temperature since no change was detected when carrying out repeated impedance diagrams at room temperature.

We also recorded impedance diagrams using Li metal non blocking electrodes for unannealed pellets. Fig. 6 shows the repeated room temperature impedance diagrams of such a $Li/Li_{10}SnP_2S_{12}/Li$ cell upon time (from t = 0 to t = 94 h). The initial diagram shows at least two

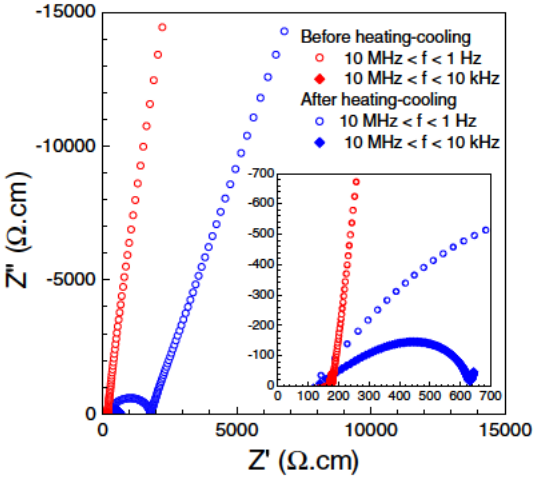

Fig. 5. Room temperature impedance diagrams of an annealed $Li_{10}SnP_2S_{12}$ pellet with sputtered gold electrodes before (red) and after (blue) the temperature cycle (RT–110 °C–RT) for two frequency sweep ranges (1 MHz–1 Hz open symbols; and 1 MHz–10 kHz solid symbols).

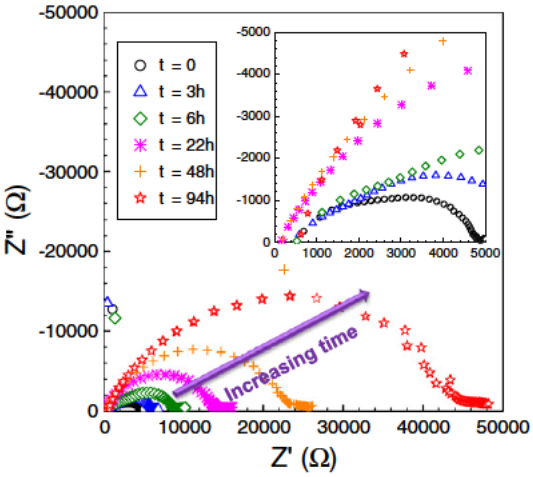

Fig. 6. Room temperature impedance diagrams of a Li/$Li_{10}SnP_2S_{12}$/Li cell vs. time.

phenomena resulting into merging semicircles, one of them being the intergrain phenomenon discussed above (see Fig. 3), and the other most probably resulting from the interface with the Li electrode. The lat ter contribution suggests that this interface is not purely non blocking as it should be for a Li + ion conductor. The striking feature is that this contribution grows very fast upon time, clearly showing that a reaction develops at this interface, and suggesting that $Li_{10}SnP_2S_{12}$ is not stable against Li even at room temperature.

3.3. Electrochemical stability

In all recent reports on sulfide solid electrolytes, the electrochemical stability is characterized by cyclic voltammetry using a pellet of solid electrolyte with a sputtered gold working electrode facing a lithium counter/reference electrode [2,4,15,18 21]. However, since the material is very likely to react with Li, the latter should be avoided as electrode.

We have therefore used a 3 electrode setup (Fig. 7a), with a sputtered gold working electrode and an Ag_3SI/Ag mixture reference electrode on one side and a larger sputtered gold counter electrode on the other side. The Ag^+/Ag^0 mixture thus realized was shown to act as a suitable comparison electrode with Li^+ conducting oxide glasses, de spite the existence of a junction potential [22]. It was further satisfacto rily used as such a reference electrode with polymeric or sulfide solid electrolytes [14,23,24]. The voltage of the reference electrode measured vs. Li metal is 2.11 V, in agreement with literature [14].

When starting the voltage sweep toward anodic values (Fig. 7b), a relatively slow current increase is observed with a leveling off until the upper limit is reached (7 V vs. Li^+/Li). During the return sweep, a very weak positive current is still measured, with no sign of reduction of what was oxidized. If one considers the often used criterion of 10 $\mu A \cdot cm^{-2}$ current density for similar sweep speeds, the anodic stabil ity of the material is only up to 2.5 V vs. Li^+/Li.

When starting with a cathodic sweep (Fig. 7c), the current density was found to increase rather fast up to 200 $\mu A \cdot cm^{-2}$ at about −0.2 V vs. Li^+/Li where the sweep was reversed. During the reverse sweep, a very sharp (re)oxidation reaction appears at a still cathodic voltage (vs. the initial rest voltage of 2.1 V vs. Li^+/Li) but significantly higher than that of the corresponding previous reduction. Upon reduction, the current density criterion is thus reached for a working electrode po tential of 1.5 V vs. Li^+/Li, with a clearly more severe reactivity than in the anodic region. When the voltage sweep is then carried on in the an odic region, an oxidation phenomenon is recorded, similar (though with lower currents) to the one observed for an initial anodic sweep (Fig. 7b). Similarly, when exploring the cathodic region after a first anodic sweep (Fig. 7b), a strong reduction phenomenon again appears, but with

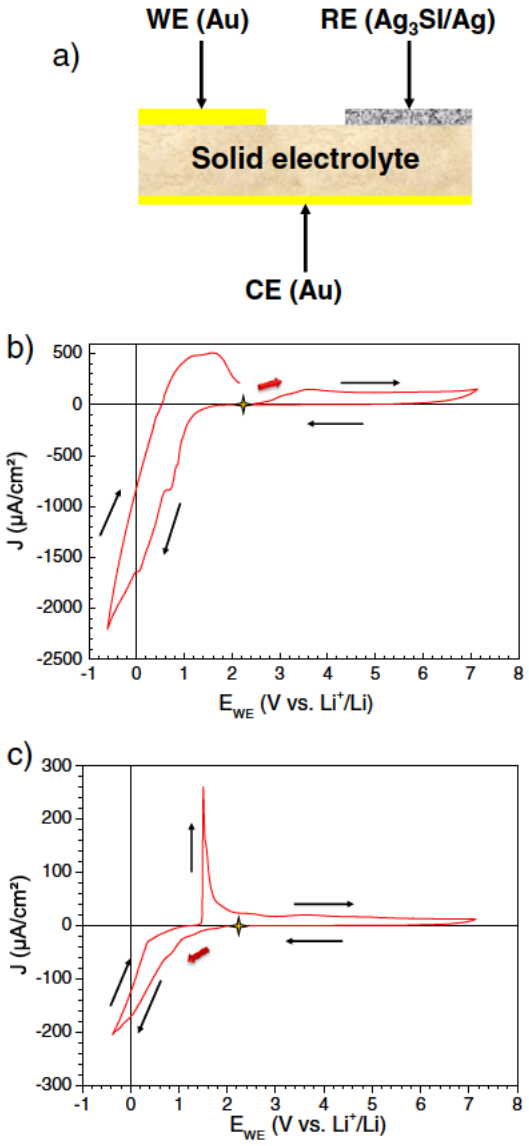

Fig. 7. a) 3-Electrode setup for electrochemical stability characterization and cyclic voltammograms of $Li_{10}SnP_2S_{12}$-NEI starting b) with an anodic sweep and c) with a cathodic sweep. Sweep speed: 20 $mV \cdot s^{-1}$.

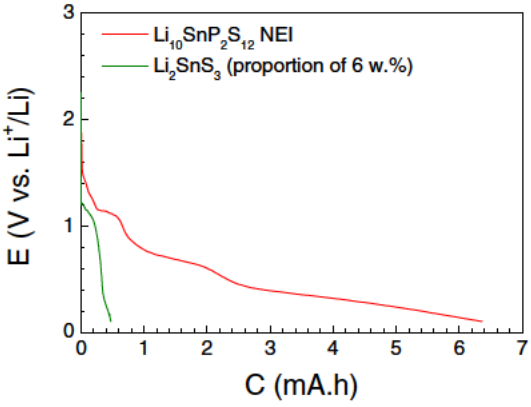

Fig. 8. Galvanostatic discharge of a Li/liquid electrolyte/$Li_{10}SnP_2S_{12}$-NEI cell (38.75 μA i.e. 1 Li in 9 h). The first discharge of Li_2SnS_3 scaled to the amount this impurity known to be present in the $Li_{10}SnP_2S_{12}$-NEI sample is also reported in green.

characteristics (in particular for the reverse sweep) somewhat different from those of an initial cathodic sweep of Fig. 7c. The last two observations are not surprising considering that the material at the working electrode is irreversibly altered by the initial reaction corresponding to the initial voltage sweep.

In order to evaluate the contribution of the Li_2SnS_3 impurity, we carried out similar cyclic voltammetry measurements on the pure sample we have synthesized. This led to very weak currents, negligible vs. the overall response of the $Li_{10}SnP_2S_{12}$ NEI sample.

Altogether, the voltammetry investigation thus reveals a very severe reduction activity of $Li_{10}SnP_2S_{12}$ at potentials below 1.5 V vs. Li^+/Li, with a reverse oxidation suggesting a different reaction. On the anodic side, oxidation starts as low as 2.5 V vs. Li^+/Li but seems to be kinetically limited, with no reverse reduction phenomenon observed.

Considering the electrochemical activity of $Li_{10}SnP_2S_{12}$ at low potential, the use of this material as an active negative electrode material is conceivable.

Liquid electrolyte coin cells were first built for $Li_{10}SnP_2S_{12}$ and Li_2SnS_3 against Li metal using 1 M LiTFSI in TEGDME/1,4 dioxane as electrolyte. Fig. 8 shows the first discharge at 38.75 μA (1 Li in 9 h) of such cells, with a scaling that allows to show the expected contribution of the known 6 wt% of Li_2SnS_3 in the $Li_{10}SnP_2S_{12}$ NEI sample. Both materials appear to react with a considerable amount of Li: 8 Li per Sn for Li_2SnS_3 and 16 Li per Sn for $Li_{10}SnP_2S_{12}$ (after deduction of the contribution from the former as impurity). This would correspond to part of the following conversion alloying reactions:

$$Li_2SnS_3 \xrightarrow{4Li} 3Li_2S + Sn \quad Sn \xrightarrow{\sim 4Li} Li_{22}Sn_5$$

$$Li_{10}SnP_2S_{12} \xrightarrow{20Li} 12Li_2S + 2Li_3P + Sn \quad Sn \xrightarrow{\sim 4Li} Li_{22}Sn_5$$

To investigate the reversibility of such processes, a careful electrode formulation would clearly be required, but this clearly confirms the strong electrochemical reactivity of $Li_{10}SnP_2S_{12}$ at low voltages. In passing, Li_2SnS_3 is also revealed to show a potentially quite interesting behavior as a conversion negative electrode, although it had been suggested to be usable as an electrolyte, despite its poorer conductivity [25].

3.4. Solid state cells

Solid state batteries were then prepared using Li_6PS_5Cl as electrolyte, which is stable vs. Li [26], a composite electrode in which $Li_{10}SnP_2S_{12}$ NEI or Li_2SnS_3 act as active material, and Li metal as negative electrode,

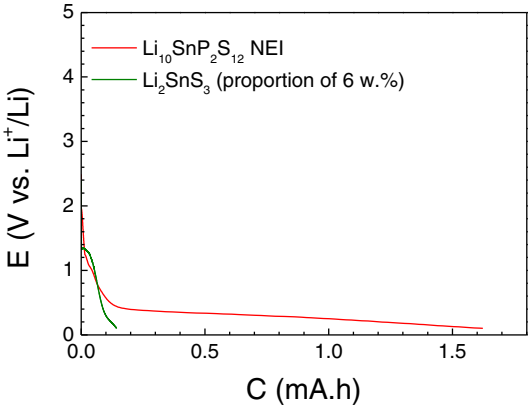

Fig. 9. Galvanostatic discharge of an $Li/Li_6PS_5Cl/Li_{10}SnP_2S_{12}$-NEI all-solid state cell (64 μA·cm^{-2} i.e. 1 Li in 3 h). The first discharge of Li_2SnS_3 scaled to the amount this impurity known to be present in the $Li_{10}SnP_2S_{12}$-NEI sample is also reported in green.

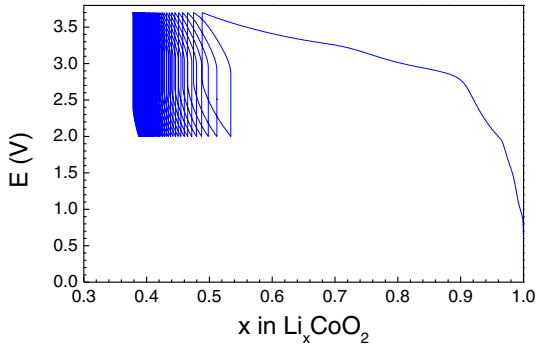

Fig. 10. Galvanostatic cycling of an $Li_{10}SnP_2S_{12}$-NEI/$LiCoO_2$ all-solid state cell (64 μA·cm^{-2} - 1 Li in 20 h).

with a pressure maintaining setup described above (Fig. 1). Fig. 9 shows the first discharge of the cells at 64 μA·cm^{-2}. Like above, the contribution of Li_2SnS_3 was plotted scaled to its amount as impurity in the $Li_{10}SnP_2S_{12}$ NEI sample. In this case, after subtracting the 0.3 mA·h contribution corresponding to the Argyrodite electrolyte and VGCF as determined in [26], the reactions correspond respectively to 5 Li per Sn for Li_2SnS_3 and to 7.5 Li per Sn for $Li_{10}SnP_2S_{12}$ NEI. Logically, stronger polarization restricts the reaction in the solid state compared to the liquid electrolyte case.

Finally, we assembled an all solid state battery using a $LiCoO_2$/$Li_{10}SnP_2S_{12}$/VGCF composite as positive electrode, $Li_{10}SnP_2S_{12}$ as solid electrolyte and a $Li_{10}SnP_2S_{12}$/VGCF composite as negative electrode. First, we checked that no detectable reaction occurs between $LiCoO_2$ and the electrolyte in the composite positive electrode: the X ray diffractogram of the mixtures shows only the lines of the components (Appendix A Fig. A2). Even though $Li_{10}SnP_2S_{12}$ is not electrochemically stable at the voltage of $LiCoO_2$, the reaction at room temperature is apparently restricted, in agreement with the shape of the voltammogram discussed above.

Fig. 10 shows that deintercalation of 0.5 lithium from $LiCoO_2$ was achieved during the first charge. If one assumes that only the part of $Li_{10}SnP_2S_{12}$ mixed with carbon (forming the potential negative electrode) reacts, this would correspond to 1.3 Li per Sn atom. This balancing of electrodes was chosen so as to investigate the concept of this in situ formed negative electrode, without pushing it to its limit of possible lithiation.

However, the subsequent discharge is clearly not possible, which is in line with the fact that such a conversion/alloying reaction cannot be expected to be reversible in the solid state considering the volume changes it must entail, at least without an elaborate electrode formulation/processing development.

Nevertheless, it is clear that the cell does not short circuit, meaning that the reaction does not propagate throughout the $Li_{10}SnP_2S_{12}$ electrolyte. Indeed, one would expect the reaction products of the lithiation, be it Li Sn alloys or more complex lithiated materials with reduced tin, to exhibit some electronic conductivity. To investigate this point more closely, we have followed the relaxation of a similar cell by opening the circuit after the charge cut off voltage was reached as shown in Fig. 11. Relaxation starts with a rapid voltage decay, but not a vertical ohmic drop type one, and continues more smoothly, which must arise from a simultaneous homogenization of the lithiation in both electrodes, and in particular to the propagation of the reaction from the negative electrode part (in contact with the current collector) to the $Li_{10}SnP_2S_{12}$ electrolyte part. Clearly, the phenomena occurring in such a cell are rather complex and not understood at this stage, but it is striking that the propagation of this reaction does not lead to short circuit as would be expected, maybe because the positive voltage of the $LiCoO_2$ electrode prevents the reaction to reach it.

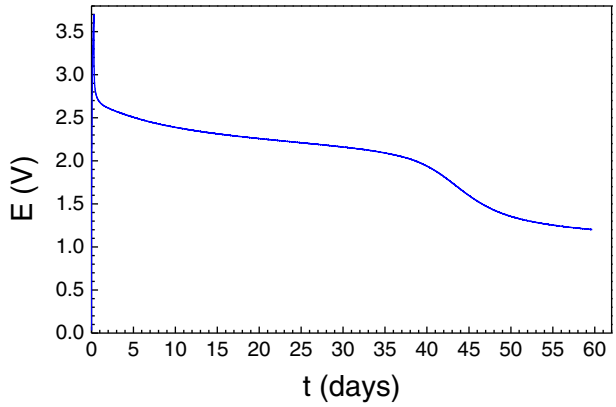

Fig. 11. Open circuit voltage evolution of a $LiCoO_2/Li_{10}SnP_2S_{12}$-NEI all-solid state cell after a first charge up to 3.7 V (64 μA·cm ^{2} - 1 Li in 20 h).

4. Conclusion

In the present study, the commercial $Li_{10}SnP_2S_{12}$ was characterized by capillary XRD. Rietveld refinement of XRD pattern shows that the material is mainly composed of $Li_{10}SnP_2S_{12}$ with the tetragonal LGPS structure, with 6 wt% of Li_2SnS_3 impurity. The refined P/Sn site occupancies correspond to a $Li_{10.03}Sn_{1.03}P_{1.97}S_{12}$ composition.

Impedance characterizations showed that annealing of $Li_{10}SnP_2S_{12}$ pellets improves the intergrain contacts, although not changing the pellet compactness. Furthermore, an interfacial or intergranular degradation was shown to result from the impedance measurements themselves, in particular at elevated temperature (110 °C) and when lower measuring frequencies are used.

Instability of $Li_{10}SnP_2S_{12}$ vs. Li was proved through impedance measurements of a $Li/Li_{10}SnP_2S_{12}/Li$ cell, with a sharp increase of its resistance with time.

A narrow electrochemical stability window was determined using cyclic voltammetry with a 3 electrode set up. Using the Ag_3SI/Ag mixture as reference electrode, we proved that $Li_{10}SnP_2S_{12}$ is unstable electrochemically especially at low potentials, contradicting very recent results by Kanno's group, based on a 2 eletrode set up with a lithium counter electrode [8,17].

Based on the instability at low potentials, we showed that $Li_{10}SnP_2S_{12}$ reacts with at least 7.6 lithium per mole according most likely to conversion and alloying reactions. Complementary Mössbauer characterization experiments are underway, which show the presence of Li Sn alloys within the $Li_{10}SnP_2S_{12}$/C electrode when submitted to voltages lower than 0.5 V vs. Li^+/Li. The Mössbauer investigation will be published elsewhere. In any case, these reactions however do not appear to be reversible in the solid state with our cell design.

Considering these ambiguous characteristics, we have also investigated the use of $Li_{10}SnP_2S_{12}$ both as negative electrode and as electrolyte, leading to a complex behavior that requires further investigation, but rather interesting in that the reaction occurring from the negative electrode side does not propagate throughout the electrolyte, and does not lead to a short circuit, at least after about 60 days.

Acknowledgment

This work was supported by the French National Research Agency, Grant No. ANR 10 LABX 0076 (Labex STORE EX).

The authors thank S. Goma for technical assistance and S. Boulineau for providing the Li_6PS_5Cl electrolyte.

Appendix A

2 Phase Le Bail refinement of $Li_{10}SnP_2S_{12}$ NEI based on a hypothetical Thio LiSICON model

Fig. A1A Le Bail full pattern matching in the Full prof suite, based on a thio LiSICON Ge type II structure ($P2_1/m$, $a = 13.396(3)$ Å, $b = 22.947(6)$ Å, $c = 18.2009(15)$ Å, $\beta = 92.562(14)°$) [4].

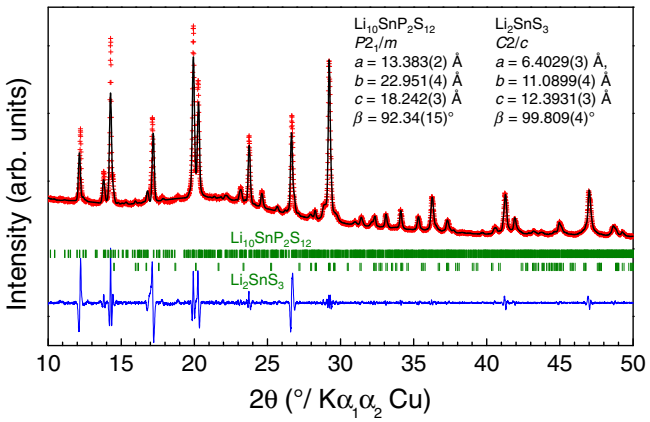

2 Phase Le Bail refinement of $LiCoO_2/Li_{10}SnP_2S_{12}$ NEI composite after 1 month

The two phases used for the refinement are $Li_{10}SnP_2S_{12}$ with LGPS structure and $LiCoO_2$.

After 1 month, no change in the lattice parameters of the 2 phases is detected ($\chi^2 = 1.29$):

$Li_{10}SnP_2S_{12}$: $P4_2/nmc$, $a = b = 8.734(2)$ Å and $c = 12.784(6)$ Å ($R_{Bragg} = 3.18\%$)
$LiCoO_2$: $R\,3m$, $a = b = 2.8155(2)$ Å, $c = 14.044(1)$ Å, and $\gamma = 120°$ ($R_{Bragg} = 3.65\%$).

Fig. A2Two phase Le Bail refinement of a $LiCoO_2/Li_{10}SnP_2S_{12}$ NEI composite electrode after one month.

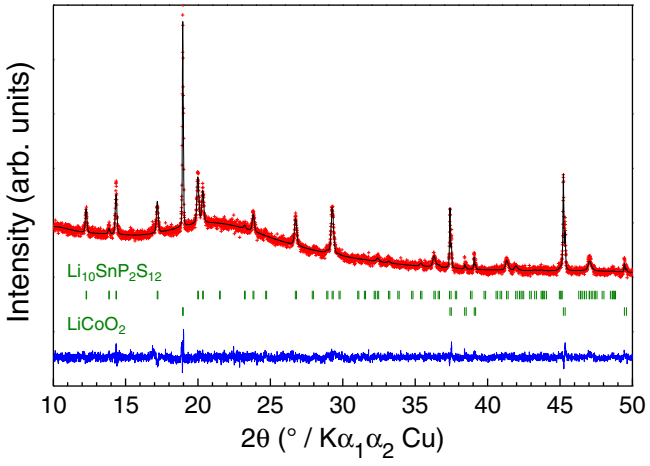

References

[1] J.M. Tarascon, M. Armand, Nature 414 (6861) (2001) 359.
[2] N. Kamaya, K. Homma, Y. Yamakawa, M. Hirayama, R. Kanno, M. Yonemura, T. Kamiyama, Y. Kato, S. Hama, K. Kawamoto, A. Mitsui, Nat. Mater. 10 (9) (2011) 682.
[3] A. Kuhn, J. Kohler, B.V. Lotsch, Phys. Chem. Chem. Phys. 15 (28) (2013) 11620.
[4] R. Kanno, M. Murayama, J. Electrochem. Soc. 148 (2001) A.
[5] Y.F. Mo, S.P. Ong, G. Ceder, Chem. Mater. 24 (1) (2012) 15.
[6] S.P. Ong, Y. Mo, W.D. Richards, L. Miara, H.S. Lee, G. Ceder, Energy Environ. Sci. 6 (1) (2013) 148.

[7] O. Kwon, M. Hirayama, K. Suzuki, Y. Kato, T. Saito, M. Yonemura, T. Kamiyama, R. Kanno, J. Mater. Chem. A 3 (1) (2015) 438.
[8] S. Hori, K. Suzuki, M. Hirayama, Y. Kato, T. Saito, M. Yonemura, R. Kanno, Faraday Discuss. 176 (0) (2014) 83.
[9] P. Bron, S. Johansson, K. Zick, J.r. Schmedt auf der Günne, S. Dehnen, B. Roling, J. Am. Chem. Soc. (2013).
[10] F. Han, T. Gao, Y. Zhu, K.J. Gaskell, C. Wang, Adv. Mater. 27 (23) (2015) 3473.
[11] A. Kuhn, T. Holzmann, J. Nuss, B.V. Lotsch, J. Mater. Chem. A (2014).
[12] J. Rodríguez-Carvajal, Phys. B Condens. Matter 192 (1–2) (1993) 55.
[13] T. Takahashi, O. Yamamota, Electrochim. Acta 11 (1966) 779.
[14] M. Menetrier, A. Levasseur, P. Hagenmuller, J. Electrochem. Soc. 131 (9) (1984) 1971.
[15] S. Boulineau, M. Courty, J.M. Tarascon, V. Viallet, Solid State Ionics 221 (2012) 1.
[16] A. Kuhn, O. Gerbig, C. Zhu, F. Falkenberg, J. Maier, B.V. Lotsch, Phys. Chem. Chem. Phys. 16 (28) (2014) 14669.
[17] Y. Kato, R. Saito, M. Sakano, A. Mitsui, M. Hirayama, R. Kanno, J. Power Sources 271 (0) (2014) 60.
[18] M. Murayama, R. Kanno, M. Irie, S. Ito, T. Hata, N. Sonoyama, Y. Kawamoto, J. Solid State Chem. 168 (1) (2002) 140.
[19] M. Murayama, N. Sonoyama, A. Yamada, R. Kanno, Solid State Ionics 170 (3–4) (2004) 173.
[20] A. Hayashi, K. Minami, M. Tatsumisago, J. Non-Cryst. Solids 355 (37–42) (2009) 1919.
[21] A. Hayashi, K. Minami, M. Tatsumisago, J. Solid State Electrochem. 14 (10) (2010) 1761.
[22] A. Kone, M. Armand, J.L. Souquet, Electrochim. Acta 27 (6) (1982) 653.
[23] M.B. Armand, M.J. Duclot, P. Rigaud, Solid State Ionics 3–4 (0) (1981) 429.
[24] J.L. Souquet, E. Robinel, B. Barrau, M. Ribes, Solid State Ionics 3–4 (0) (1981) 317.
[25] J.A. Brant, D.M. Massi, N.A.W. Holzwarth, J.H. MacNeil, A.P. Douvalis, T. Bakas, S.W. Martin, M.D. Gross, J.A. Aitken, Chem. Mater. (2014).
[26] S. Boulineau, Synthèses et caractérisations de matériaux céramiques, vitreux et vitrocéramiques à base de soufre, utilisables comme électrolytes dans les Batteries « Tout-Solide ». (PH-D Thesis), University Picardie-Jules Verne, 2013 https://tel.archives-ouvertes.fr/tel-01356443.